Soft Matter

RSC Publishing

PAPER

Biopolymer gels with "physical" cross-links: gelation kinetics, aging, heterogeneous dynamics, and macroscopic mechanical properties

Cite this: *Soft Matter*, 2013, **9**, 3931

Eleonora Secchi,*[a] Tommaso Roversi,[b] Stefano Buzzaccaro,[a] Laura Piazza[b] and Roberto Piazza*[a]

Received 18th September 2012
Accepted 5th February 2013

DOI: 10.1039/c3sm27153f

www.rsc.org/softmatter

Alginate is a natural biopolymer that forms, in the presence of divalent cations, ionic-bound gels typifying a large class of biological gels stabilized by non-covalent cross-links, and displaying a consistent restructuring kinetics. We investigate the kinetics of formation and aging of alginate gels by slow permeation of a curing $CaCl_2$ agent by means of photon correlation imaging, a novel optical technique that allows obtaining the microscopic dynamics of the sample, while retaining at the same time the spatial resolution of imaging techniques. Specifically, the gelling kinetics displays a peculiar non-diffusive behavior, and the subsequent restructuring of the gel structure shares several features in common with the aging of colloidal gels, in particular for what concerns the occurrence of heterogeneous dynamics effects. A comparative analysis of the gel macroscopic mechanical properties at different aging stages further highlights distinctive effects arising from the non-permanent nature of the bonds.

1 Introduction

Understanding the connection between the microstructure and the mechanical properties of polymer hydrogels, which constitute a basic structural component of living cells, of the extracellular matrix, and in general of most soft biological tissues, is of primary importance in view of their increasing use in the field of biomaterials.[1] The most striking feature of these systems is the gamut of elastic and rheological effects they exhibit under stress, ranging from full fluidization to strong reinforcement.[2–4] The microscopic property commonly credited to be at the roots of this rich behavior is due to the distinctive nature of the gel cross-links that, at variance with the case of simple polymer gels, can usually break and re-form at a different location, either spontaneously or under the effect of minute changes of the surrounding environment. The reversible binding of specific cross-linking proteins, allowing us to tune not only the gel mechanical properties but also the relevant time-scales in which these changes take place, has been for instance proposed as the basic mechanism mediating between fluidization and reinforcement of the cytoskeleton subjected to a mechanical stimulus.[5–8]

The opportunity of tuning the rheological properties of gels with reversible cross-links, lying somehow in between chemical and physical gels, is quite promising for technological applications. For instance, in the field of regenerative medicine, long-term application of cyclic strain has already been found to enhance the mechanical properties of engineered muscle tissues.[9] Exploiting in full the peculiar features of biological hydrogels requires however a clear understanding of the relationship between microscopic cross-link dynamics and macroscopic mechanical properties using simple model systems, which the complex hydrogels formed by protein biopolymers in living systems rarely are. The main aim of this paper is to show that substantial information can be obtained by studying common polysaccharide hydrogels extensively used in the food industry to ameliorate texture, stability, or mouth feel, and in more advanced applications such as the formulation of nutraceuticals providing health and medical benefits.[10] Among this wide class of natural biopolymers, which include traditional foodstuff such as starch and pectins, an increasingly important role is taken by alginate, actually a family of unbranched polysaccharides isolated from brown seaweeds, which is one of the extensively used materials in tissue engineering,[11] for immobilizing living cells[12] and, recently, to obtain, when mixed with polyacrylamide, highly stretchable composite gels.[13] Structurally, alginates are block copolymers composed of β-D-mannuronic acid (M) and α-L-guluronic acid (G) arranged in a blockwise pattern where homopolymeric regions of M (M-blocks) and G (G-blocks) residues are interspersed by regions of alternating structures (GM-blocks).[14] The addition of divalent cations such as Ca^{2+}, which can be hosted within molecular cavities ("egg-boxes") formed by repeating G-blocks, can drive the formation of ionic gels[15] by binding negatively charged oxygen atoms belonging to two adjacent alginate chains. This simplified

[a]*CMIC, Dipartimento di Chimica, Materiali e Ingegneria Chimica, Politecnico di Milano, 20133 Milano, Italy. E-mail: roberto.piazza@polimi.it*

[b]*DeFENS, Dipartimento per gli Alimenti, la Nutrizione e l'Ambiente, Università di Milano, 20133 Milano, Italy. E-mail: laura.piazza@unimi.it*

"egg-box" model has recently been questioned, since GM blocks too are found to contribute to chain cross-linking, albeit to a lesser extent.[16] All evidence suggests anyway that alginate gels are held together by non-covalent bonds primarily due to ion bridging, although hydrogen bonds and dispersion forces may also contribute to the gel strength.[17] At variance with the chemical bonds in simple polymer gels, these "physical" cross-links are prone to break and re-form to relax local internal stresses that build up upon gelation. Such a non-permanent, reversible nature of the cross-links is very likely to be responsible for the thermo-reversibility of alginate gels and for their propensity to display creep behavior over long times.[16,17] Moreover, the macroscopic properties of the gel are expected to depend not only on the density, strength, and lateral extent of the cross-links, but also on their restructuring kinetics.[18,19]

Rheological studies of alginate gels are most commonly performed in the linear region of small deformations, which is adequately described by usual viscoelastic models, and where the Young's modulus is typically used as a measure of gel strength. Unfortunately, in most interesting applications the samples are subjected to strains well beyond the linear regime, which can result in a very complex behavior brought in by the interplay between structure and its evolution through junction binding/unbinding.[20]† Recent experimental findings concerning cell biomechanics suggest that concepts borrowed from soft glass rheology may fruitfully account for some basic features of the nonlinear rheological behavior of biopolymer gels. In this conceptual framework, the system temporally evolves into a complex energy landscape characterized by a large number of local minima, with a typical depth larger than the thermal energy. Hence, moving in this complex landscape requires an activation energy related to an "effective" or "noise" temperature[8] whose microscopic origin has been shown, in the case of bundled cytoskeletal networks, to be related to frozen internal stresses promoting local rearrangement events.[6]

In this paper, through a detailed investigation performed by photon correlation imaging, a novel light scattering technique particularly suitable to investigate the microscopic dynamics of spatially inhomogeneous systems, we highlight and discuss several features of the gelation kinetics and the restructuring processes in alginate gels generated by the slow perfusion of $CaCl_2$.[22] In particular, the advancement of the gelation front, accurately marked by a dramatic increase of dynamic time correlations, displays a very surprising, non-diffusive time behavior, which can hardly be reconciled with the existing gelation model. After the formation of a dynamically quasi-arrested structure, the gel undergoes a time evolution characterized by a first consistent restructuring and strengthening accompanied by a progressive slowing-down of the local dynamics, followed by a much longer period marked by drastic and abrupt global "fluidization" events, which do not apparently lead to significant changes of the gel structure, but presumably contribute to a slow "creeping" behavior observed for the gel at very long time. Finally, the macroscopic mechanical properties of the gel show evident traces of the temporal evolution analyzed by PCI, giving experimental evidence that alginate gels share many properties in common with attractive colloidal glasses. Our results therefore suggest that the physical mechanisms that are supposed to account for the mechanical and rheological properties of soft glassy systems may have a wider generality, and may be shared by polymer gels with physical cross-links.

† This is for instance the case of a recently developed method for controlled release from drug-loaded alginate hydrogels based on suitable control of the time-response to applied stresses.[21]

2 Materials and methods

2.1 Alginate samples

Sodium alginate (Algogel 6020) was obtained from Cargill Inc., France, and used without further purification. The mannuronic and guluronic weight fractions within this specific alginate are reported in Table 1, which also shows the fractional amount of the homo- and hetero-bonds between the two monomer units, whose values strongly influence the gelling process. Size exclusion chromatography[23] yields a polymer number-averaged molecular weight $M_n \simeq 110$ kDa, corresponding to a degree of polymerization of about 200, and a weight-averaged molecular weight $M_w \simeq 330$ kDa. Hence, this natural biopolymer displays a very large degree of polydispersity $M_w/M_n \simeq 3$. Alginate solutions at a polymer weight fraction of 2% were prepared by dissolving solid Na^+-alginate in the desired volume of deionized water containing 0.02% (w/w) sodium azide to prevent microbiological growth, and gelation was induced by slowly permeating them with $CaCl_2$ according to the protocols described in what follows.

2.2 Photon correlation imaging

Photon Correlation Imaging (PCI) is a recently introduced optical method, suitable to investigate slow dynamics in colloidal glasses and gels by measuring the time-correlation function of the scattered light, as in standard Dynamic Light Scattering (DLS), but with the major advantage of allowing for spatial resolution by investigating the *local* dynamics at distinct points within the scattering volume. We shall give only a summary description of PCI, mainly emphasizing the rich amount of physical information that can be extracted using this powerful technique, and referring to the seminal contributions by L. Cipelletti and coworkers for a more detailed analysis.[24,25] Basically, the experiment consists of forming on a multi-pixel camera an image of the scattering volume, observed at a given scattering angle ϑ, through a suitably stopped-down optics (see Fig. 1a). In other words, the imaging optics is provided with a partially closed iris diaphragm placed in the focal plane of the

Table 1 Mannuronic (X_M) and guluronic (X_G) weight fractions in Algogel 6020, and weight fractions of the dimeric units X_{GG}, X_{GM+MG} and X_{MM}. Data have been obtained according to the method described in ref. 23

X_G	X_M	X_{GG}	X_{GM+MG}	X_{MM}
0.56	0.44	0.26	0.60	0.14

lens that, besides accurately selecting the scattering wave-vector $q = (4\pi/\lambda)\sin(\vartheta/2)$, causes the image to become "speckled" because the intensity at each given point on the image plane originates from the interference of the field scattered by a finite-size region in the sample plane. The simultaneous measurement of the time-dynamics over many speckles yielded by the multi-pixel detector, besides providing a fast ensemble averaging of the intensity correlation function (crucial when investigating samples with a very slow dynamics), allows us to identify the occurrence and follow the temporal evolution of those dynamic effects associated with the presence of spatial heterogeneities in the investigated sample. Quantitatively, the latter can be characterized as follows. First, the speckle pattern is subdivided into "regions of interest" (ROIs) by grouping together a given number of adjacent pixels. Then, one introduces the so-called "degree of space–time correlation" (or "correlation index") $c_I(\tau;t,\boldsymbol{r})$ between two images taken at times t and $t + \tau$ as

$$c_I(\tau;t,\boldsymbol{r}) = \frac{\langle I_p(t) I_p(t+\tau)\rangle_{\boldsymbol{r}}}{\langle I_p(t)\rangle_{\boldsymbol{r}} \langle I_p(t+\tau)\rangle_{\boldsymbol{r}}} - 1 \quad (1)$$

where I_p is the scattered intensity measured by the p^{th} pixel and $\langle\cdots\rangle_{\boldsymbol{r}}$ denotes an average over all pixels within a ROI centered around $\boldsymbol{r}$. Hence, $c_I(\tau;t,\boldsymbol{r})$ is simply related to the covariance between the intensity measured on the same speckle at two different times, sampled over the given ROI and, in particular, $c_I(0;t,\boldsymbol{r})$ is the relative variance of the intensity in $\boldsymbol{r}$ at time t. Note that c_I is a function of the delay time τ that, in samples displaying a restructuring and aging kinetics, depends parametrically on the aging time t (and, for spatially inhomogeneous samples like those considered in this work, also on the local position $\boldsymbol{r}$). In fact, as shown in what follows, it is exactly this time-dependence that yields the basic features of the gelation process. Provided that the investigated kinetics is sufficiently slow, however, the statistical accuracy can be enhanced by time-averaging $c_I(\tau;t,\boldsymbol{r})$ over a time window δt that is much shorter than the characteristic evolution time of the investigated kinetics, which allows us to reduce the statistical noise due to finite sampling on the limited number of pixels in a ROI. The local dynamics can then be quantified by defining‡

$$g_2(\tau) - 1 = \langle c_I(\tau;t,\boldsymbol{r})\rangle_{\delta t}. \quad (2)$$

Such a "coarse-grained" correlation index actually bears the same information of the intensity correlation function measured in a standard DLS experiment, yet with the crucial advantage of a much better statistical accuracy due to pre-averaging over the speckles in a ROI, which allows averaging over a time window δt much shorter than the total measurement time required in a DLS measurement.

In glassy or gelling systems, however, the correlation index also displays *intrinsic* fluctuations, which are not just due to the instrumental noise associated with finite-sampling, but to real physical processes taking place in the system. A striking manifestation of these physical fluctuations on which we shall particularly focus is the occurrence of sudden "correlation bursts" due to structural rearrangements that rapidly propagate over large regions of the sample. Such a "dynamic heterogeneity" can be investigated by considering the (coarse-grained) variance of $c_I(\tau;t,\boldsymbol{r})$ on a ROI

$$\chi(\tau) = \langle c_I(\tau;t,\boldsymbol{r})^2\rangle_{\delta t} - \langle c_I(\tau;t,\boldsymbol{r})\rangle_{\delta t}^2 \quad (3)$$

which quantifies the temporal evolution of the restructuring events taking place at a given location and aging time. As shown in the above equation, the dependence of $\chi(\tau)$ on the delay τ allows us to easily set apart slow changes of the local dynamics associated with aging from the aforementioned sudden global restructuring events. Whereas the former processes are indeed characterized by a peak in the local value of χ occurring at a delay time τ comparable to the relaxation time of $g_2(\tau)$ and getting more pronounced the larger the size of the correlated region within the sample,[26] the latter are highlighted by a sudden increase of $\chi(\tau)$ over the whole sample which is not correlated with the local dynamics.

What is also particularly interesting for the present study is that PCI, besides being a sensitive probe of the dynamic slowing-down and kinetic arrest associated with gelation, also allows us to detect and map the presence of hydrodynamic motion in the sample. Indeed, whereas standard DLS can detect only *relative* particle motion (in other words, provided that the scattering volume is uniformly illuminated, the far-field speckle pattern generated by a system of scatterers in uniform motion remains stationary), in a PCI configuration the speckle motion on the image plane faithfully maps the local flow field within the sample. As in standard Particle Imaging Velocimetry (PIV[27]) techniques this allows us to obtain *via* a FFT algorithm the spatial cross-correlation function of the speckle pattern at

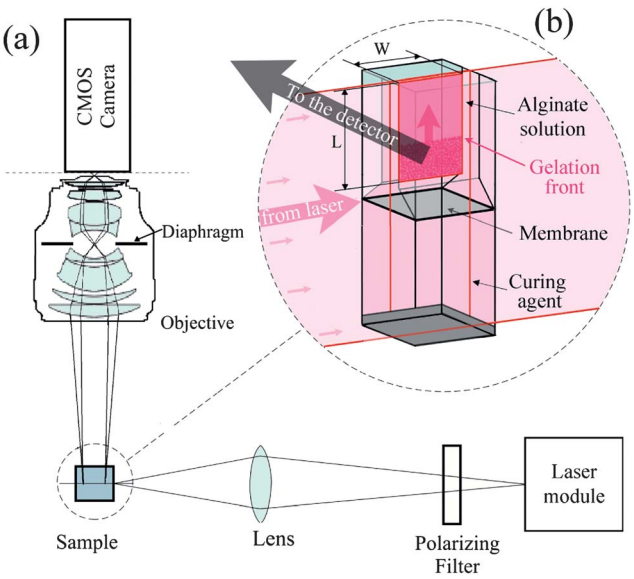

Fig. 1 (a) Scheme of the PCI setup in a 90° scattering angle configuration. (b) Scheme of the optical cell used to perform gelation.

‡ To simplify this notation, we leave out the parametric dependence of $g_2(\tau)$ on t and $\boldsymbol{r}$, which is however to be understood.

different times t_1 and t_2. In this scheme, the local sample displacement in the time interval $t_2 - t_1$ is related to the position of the cross-correlation peak, whereas the height of the peak itself decays on a time scale set by the Brownian dynamics of the sample measured at a wave-vector q. This technique, which has been successfully used to probe the collapse and restructuring of colloidal depletion gels,[22] proves to be extremely useful for investigation of the detailed mechanism by which gelation proceeds.

To follow gelation, the alginate solution is confined to the lower, optically accessible part of a cuvette (VWR International), by a porous membrane with 100 μm pore size, which is mounted on a custom-made plastic frame that tightly fits into the wedge-shaped connection between the sample compartment and an upper reservoir (see Fig. 1b). This cell geometry allows us to laterally image a rectangular area S within the sample with a vertical extent $L \simeq 16$ mm and a horizontal width $W \simeq 6.4$ mm, which allows mapping the sample region extending from the cell bottom down to about 3.5 mm over the membrane (in the following, we call z the vertical distance from the bottom of S). Gelation is started by gently pouring the curing agent (a 0.1 M $CaCl_2$ solution) in the reservoir atop the membrane, carefully avoiding the presence of air bubbles. The cell is then rapidly turned upside down and mounted on the cell holder with the reservoir at the bottom to avoid convection effects that may arise from the fact that the $CaCl_2$ solution is slightly denser than the alginate fluid (see also Section 3.2). The illumination optics is composed of a 50 mW semiconductor laser module operating at $\lambda = 656$ nm (SY Lasiris SNF501L, StockerYale, New Hampshire, USA) that includes a holographic grating allowing us, with the aid of a lens ($f = 300$ mm), to shape the beam on the cell entrance window as a uniform vertical sheet of width $w = 20$ mm (see Fig. 1a). An objective images the investigated sample region S on a rectangular area with a size of 300 px × 120 px of a CMOS camera sensor (Optikam Pro5, Ponteranica, Italy), whereas a diaphragm placed in the objective focus selects a scattering angle $\vartheta = 90°$ (corresponding to a scattering wave-vector $q \simeq 1.8 \times 10^5$ cm^{-1}) with a speckle size of about 3 px × 3 px. The exposure time is typically set to 1/15 s, with a time interval between successive images of 30 s, and the sensor gain is tuned during the gelation process so as to optimize the intensity of the speckle pattern within the gel phase. Since during the gelation kinetics the intensity and correlation index are expected to depend only on the vertical position z, the speckle pattern image was subdivided into 30 ROIs with a height of 10 px (corresponding to about 530 μm in the sample) and laterally extending over the whole width W of the investigated sample region (120 px). Each ROI contains therefore about 100 speckles, a value which was found to yield a good vertical resolution with an acceptable statistical noise in the correlation function. If necessary, spatial resolution can nonetheless be simply improved by changing the imaging lens and focusing on a smaller gel region. Finally, the space–time resolved correlation index $c_I(\tau;t,\boldsymbol{r})$ is then computed for each ROI using a custom-made code running on ImageJ, a public domain image processing software.

2.3 Mechanical tests

To investigate the macroscopic mechanical properties of alginate hydrogels, several gel samples were prepared by pouring the liquid solution of alginate into dialysis tubes with a diameter of 21 mm (Sigma Aldrich, MWCO 12 000) and an overall length of 200 mm, which were then sealed and immersed in a water bath containing a 0.1 M calcium chloride solution. To detect the effects of microscopic restructuring observed by PCI on the gel macroscopic properties, the samples were extracted in sequence from the gelation bath after a curing time increasing from 6 hours up to 6 days. Each cylinder was transversally cut into cylindrical sections, which were then separately subjected to uniaxial compression tests using a texture analyzer TA (XTplus, Stable Micro System, England) operating at $T = 23$ °C. To eliminate any effect due to the non-ideal cutting of the cylinders, the samples are sandwiched between the upper and lower plates of the TA, and first pre-loaded with a stress of about 2–3 kPa, so as to compress them to a length h_0 which is about 2% smaller than the unperturbed value. Measurements then consist of further compressing them at a minimum constant speed of $V = 1$ mm s^{-1} from an initial height h_0, accurately measured after the pre-stress has been applied, up to rupture. To check for reproducibility, tests were repeated on several samples for each value of the time spent in the gelation bath. To obtain the stress relaxation curve behavior, similar cylindrical gel samples were submitted to a quasi-static uniaxial compression at constant deformation, and the stress recorded as a function of time for a maximal duration of about 1 h. The initial deformation was applied at the very high strain rate of 33 mm s^{-1}, allowing us to consider it as quasi-instantaneous.

3 PCI analysis of the gel formation and aging

3.1 General features of the gelation process

A preliminary qualitative description of the progress of the gelation process permits us to single-out its main features and set apart distinct time regimes, allowing us at the same time to familiarize with the kind of information that can be extracted from a comparative analysis of the intensity and degree of correlation profiles obtained by PCI. With a negligible delay, due to the time it takes to cross the separating membrane, the curing agent that has been poured into the lower compartment of the cell starts diffusing into the upper compartment, triggering the onset of alginate gelation and generating a gelation front that propagates upwards, as shown by the three snapshots in Fig. 2. Visually, this front is marked by a noticeable increase of the scattered intensity in the cell region already invaded by the $CaCl_2$ solution.

This effect can be related to the microscopic dynamics of the gelling alginate solution by contrasting the time behaviour of the scattered intensity and the correlation index on a *single* ROI of the sample, located at $z = 5$ mm from the cell bottom (namely, approximately 8 mm above the membrane). Fig. 3 shows that at $t_0 \simeq 24$ h, roughly corresponding to the time it takes for the curing solution to propagate from the membrane

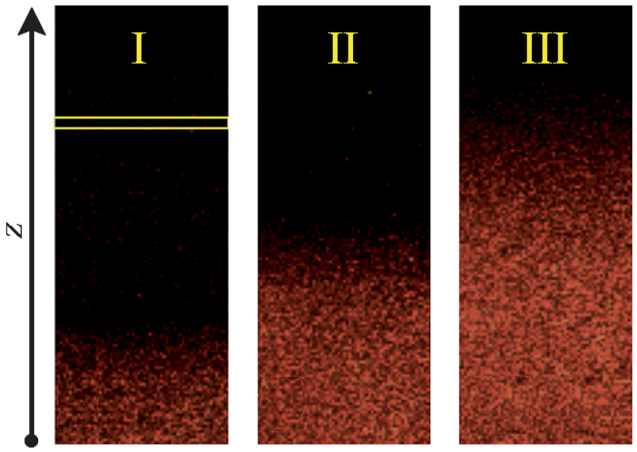

Fig. 2 Snapshots of the cell taken about 13 (I), 25 (II), and 45 (III) hours after the curing agent has been poured into the reservoir. The z axis indicates the measurement coordinate, whereas the yellow box indicates the size and shape of a ROI.

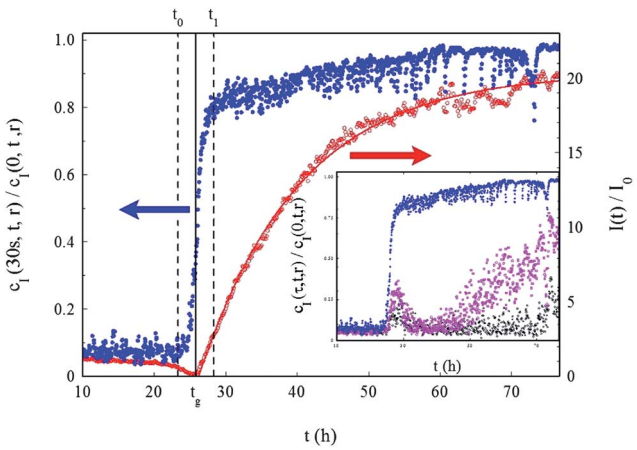

Fig. 3 Time dependence of the intensity ratio $I(t)/I(0)$ (open dots, right axis) and the normalized degree of the space–time correlation $\hat{c}_I(\tau,t,z)$ after a delay of $\tau =$ 30 s (bullets, left axis), measured for a ROI centered at $z = 5$ mm. The full line is an exponential fit to the intensity curve for $t > t_g$ with a time constant $t_a \simeq 850$ s. The inset shows the normalized correlation index at delay times $\tau = 10$ min and $\tau =$ 50 min.

up to the ROI location, after an initial dip the scattering intensity starts to grow, reaching a plateau which is about 20 times larger than its value at $t = 0$. The rising part of the intensity is rather well fitted by an exponential with a time constant $t_a \simeq 850$ s. Since an increase of the scattering intensity witnesses a change in the sample structure factor,§ this means that structural rearrangements keep on taking place in the ROI for a long period of time, quantified by the "aging" time t_a.

The temporal evolution of the local microscopic dynamics is, however, very different. To highlight this contrasting behavior, it is useful to introduce a "normalized" degree of correlation by taking the ratio $\hat{c}_I(\tau;t,z) = c_I(\tau;t,z)/c_I(0;t,z)$ of $c_I(\tau;t,z)$ to its value at $\tau = 0$.¶ Let us first concentrate on the behavior of $\hat{c}_I$ for shortest delay time $\tau = 30$ s between two images of the ROI. Since the decay time of the correlation function for a fluid alginate solution, measured by standard DLS at the same q-vector, is of about 25 ms, it is not surprising that, for $t < t_0$, the correlation index between the two speckle patterns is basically zero. However, as soon as the scattered intensity starts to change, $\hat{c}_I(\tau,t,z)$ shows a rapid increase, reaching a value of about 0.9 in a few minutes. In other words, for $t > t_1$ the speckle pattern is still fully correlated after a delay time that is more than two orders of magnitude longer than the correlation time of the alginate solution. Hence, for $t > t_1$, the whole alginate solution in the ROI is already a quasi-arrested gel, where however noticeable structural rearrangements, highlighted by the persisting increase of $I(t)$, are still going on. Noticing that $t_1 - t_0$ is of the order of magnitude of the time it takes for the Ca^{2+} ions to traverse the ROI, the conversion of the solution into a dynamically arrested structure can be assumed to take place almost instantaneously when the curing agent becomes available. Such a sharp dynamic arrest allows us to take $t_g = (t_0 + t_1)/2$ as a reasonable average time in the ROI marking the transition from a fluid to a gelled system. By *quasi*-arrested, however, we mean that residual dynamic effects persist in the gel well beyond t_g. The inset in Fig. 3 shows indeed that the degree of correlation still decays over *much* longer delays. Indeed, after a delay of $\tau = 50$ min, $\hat{c}_I(t)$ has decreased to zero even at a time t when $I(t)$ has basically reached its plateau value. If at this stage structural changes are associated with such a long-time decay of the correlations, they are too weak to be mirrored by changes in the scattering intensity at the selected q-vector. Actually, we have not detected a fully arrested dynamics after *any* ripening time. An investigation of the macroscopic stress relaxation discussed in Section 4 shows that such a long persistence of diffusive microscopic dynamics is arguably responsible for a slow macroscopic creeping of alginate gels.

3.2 Kinetics of the gelation front

The abrupt increase of c_I suggests that dynamic arrest, or at least a dramatic increase of the correlation time imputable to the formation of a loose gel structure, is a quasi-instantaneous process, taking place as soon as Ca^{2+} comes into contact with alginate. The time-dependence of the advancement of the gelation front along the cell, tracked by plotting the "gelling time" t_g for each single ROI, is however quite surprising. Fig. 4 shows that the gelation front advances indeed *linearly* with time with a speed of $v_g = z(t_g)/t_g \simeq 0.3$ mm h^{-1} over the whole investigated range. Extrapolated to $t_g = 0$, the linear fit yields $z = -2.8$ mm, which is consistent with the estimated position of the membrane. Note also that the time $t_1 - t_0$ it takes for c_I at a delay time of 30 s to switch up to a value close to one is approximately constant and in good agreement with the time it takes for the gelation front to cross a ROI at the constant speed v_g.

§ Reflecting a progressive increase of the size of the correlated scattering regions, provided that they do not get so large that the scattering pattern becomes strongly forward-peaked.

¶ This procedure may be reasonably expected to get rid of most of the statistical fluctuation associated with the finite pixel sampling and to better highlight the physical contribution due to local restructuring processes.[28]

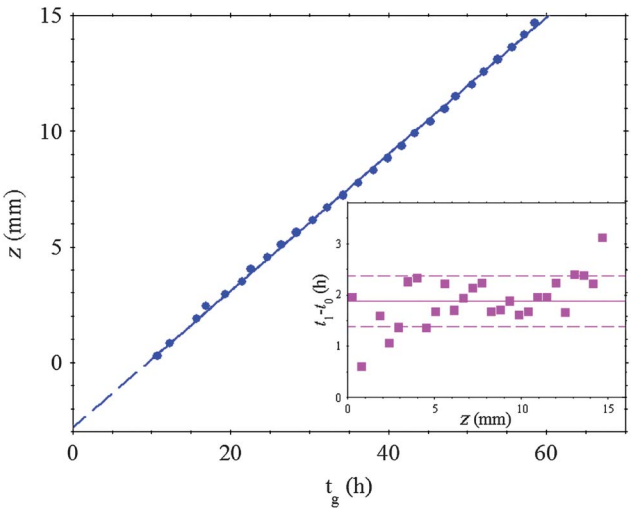

Fig. 4 Kinetics of the gelation front, showing the position z corresponding to a specific gelling time $t_g = (t_1 + t_0)/2$. The linear fit yields an advancing speed $v_g \simeq 0.3$ mm h^{-1}, and an intercept $z(0) \simeq -2.8$ mm, approximately coincident to the position of the separating membrane. The inset shows that $t_1 - t_0$ is almost independent from the position in the cell, roughly amounting to the time it takes for the gelation front to traverse a ROI at the constant speed v_g (here full and broken lines indicate the average value and standard deviation of $t_1 - t_0$).

This striking experimental evidence can hardly be reconciled with the existing models of alginate gelation. The most widely used approach, due to Mikkelsen and Elgsaeter (M–E model[29]), is indeed based on assuming that the local concentration of both calcium ions and free alginate behaves diffusively, decreasing at the same time because of the formation of the polymer gel. The latter is conversely assumed to be immobile, with a local concentration that steadily grows because of two different mechanisms, the inclusion of an additional monomer to an already formed network and the novel association between two free chains. For a generic dependence of the diffusion coefficients on the concentration of the three species, these assumptions lead to a set of nonlinear equations that must be solved numerically.[29] However, within the (strongly) simplifying assumption of constant diffusion coefficients of alginate and calcium ions, the M–E model becomes just a particular case of a reaction–diffusion process, which has been extensively investigated in the literature because of its large interest both in chemical and biological pattern formation[30] and in the context of diffusion limited aggregation[31] with sophisticated methods.[32–35] When applied to gelation, these analytical solutions yield a gelation front position $z_f(t)$ that, for initially separated reagents at concentrations a_0 and c_0, behaves *diffusively*, $z_f^2(t) \xrightarrow[t\to\infty]{} D_f t$, with a long-time front diffusion coefficient D_f that can be evaluated by equating the fluxes of the reactants at the position of the gelation front.[35]

Whereas a suitable dependence of the diffusion coefficients on the concentration of the reacting species may lead to a time behavior which is not strictly diffusive, as observed in other experiments,[36,37] it is much harder spotting a clear physical mechanism yielding a gelation front that, instead of a diffusing, propagates at a constant speed along the cell. A possible explanation may be hinted by the initial moderate decrease in intensity which is detected just in the region where c_I starts to grow (namely, close to the leading edge of the gelation front, see Fig. 3), which is observed to a greater or lesser extent for all the ROIs. Such a dip in the scattered intensity may reasonably be attributed to the presence of a thin layer before the advancing gel, with a thickness of the order of a few hundred microns, where the concentration of alginate is sensibly lower than in the bulk. The physical origin of such a "depletion layer", which has apparently been observed in other measurements of alginate gelation,[37,38] is not easy to spot. Tentatively, we suggest that it could stem from a mechanism that is not included in the M–E model: syneresis, namely a progressive shrinking over long times of the structure by solvent ejection, which is a common and extensively studied phenomenon in polymer gels. In the investigated sample, syneresis of the alginate matrix is already highlighted for times slightly exceeding the gelation time of the whole sample by the onset of a slow uniform translation of the speckle field, witnessing a *backward* motion of the whole gel structure towards the negative z direction, which eventually leads, at much longer times, to gel detachment from the cell bottom and lateral walls. However, gel shrinking is very likely to take place even before, *while* the gelation front advances and the gel gets progressively reinforced by the increase in the cross-link density supplied by the incoming Ca^{2+} ions. Since the diffusion constant of alginate is very low, this might presumably leave a polymer-depleted region just on top of the gel.‖

Whether or not this physical mechanics is plausible, the presence of the depletion layer implies that there is a region within the sample where the density profile of the solution gets *inverted*, regardless of whether the alginate or the curing solution is initially placed on top. Such an inverted density profile is hydrodynamically instable, unavoidably leading to micro-convective effects. The latter, however slow, would noticeably modify the spatial distribution of the curing agent, leading in general to a quasi-uniform concentration profile within the depletion layer. The presence of convective flow is commonly expected and often experimentally observed to accelerate transport processes with respect to their purely diffusive limit.[40] Micro-convection within the depletion layer may thus lead to a very different time behavior of the gelation front.[38] To support this view, we tried to *enhance* convective effects by repeating the same experiment, but without turning the cell upside down, so that the heavier curing solution lies *on top* of the alginate solution. Fig. 5, where the times t_2 required for the scattering intensity to double its initial value (which is just slightly longer than t_g) are compared, shows that in the presence of macroscopic convection,** the time it takes for the scattered intensity

‖ Further effects which are not provided for by the M–E model may be related to the presence of an osmotic unbalance at the gel front, where the local ionic strength shows a steep gradient. In colloidal suspensions, salinity gradients are known to generate Donnan effects, which affect for instance particle diffusion or sedimentation.[39] Whether similar effects occur during the formation of an ionic polymer gels is surely a question that deserves further investigation.

** In PCI measurements, the latter is clearly highlighted by the observation of slow convective rolls traced by residual dust particles in the liquid alginate phase.

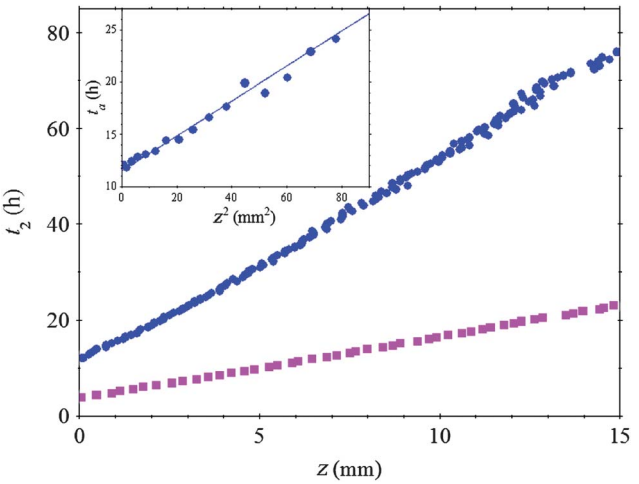

Fig. 5 Time t_2 required for the scattered intensity to double its initial value, as a function of the position in the cell, for the sample discussed in the text (bullets), and for an identical sample placed in the cell mounting with the reservoir containing the curing agent at the top (squares). The inset shows the dependence of the aging time t_a, obtained from an exponential fit to the growth of the scattered intensity curve, on the square of the measuring coordinate z.

to double its initial value linearly depends on the position z, yet the front advances with a speed that is more than three times larger than in the hydrostatically stable case. This evidence, although far from being conclusive, shows that convective effects, which are not considered in the simple diffusion/reaction model, may drastically change the time behaviour of a gelation process. This observation may be relevant in most practical applications of alginate, where the adopted geometry implies *horizontal* concentration gradients, unavoidably leading to convection.

Nonetheless, effects related to the spreading of the advancing front of the curing agent can be detected by looking at the aging time t_a, defined like in Section 3.1 as the time constant of the exponential growth of the scattered intensity at a given position z. The inset in Fig. 5 shows indeed that t_a grows quadratically with z from a minimum value $t_{a_0} \simeq 11.5$ h at $z = 0$. Such an increase can be reasonably attributed to a delay in the supply of the additional Ca^{2+} ions required for the loose percolating structure formed at t_g to "ripen". Fitting the curve as $z(t) = \sqrt{\tilde{D}(t_a - t_{a_0})}$ actually yields a fit parameter $\tilde{D} \simeq 1.7 \times 10^{-5}$ cm^2 s^{-1}, which has the typical order of magnitude of the diffusion coefficient of small ions. This rather strange combination of a linearly advancing gelation front with a gel aging that shows evident traces of the ion permeation of an already gelled structure points out the need for further studies of the kinetics of gelation processes in gels with ionic cross-links.

3.3 Gel aging

The progressive change in the gel dynamics during the restructuring period following t_g can be quantitatively analyzed by means of the correlation functions defined in eqn (2), using a coarse-graining time interval of $\delta t = 100$ min that, as shown below, is still much shorter than the aging time scale of the gel.

Fig. 6 shows that all correlation functions $g_2(\tau) - 1$ obtained on a ROI located at $z = 0.5$ mm eventually decay to zero regardless of the aging time, confirming that the gel dynamics is *never* fully arrested. The semi-logarithmic plot in the inset shows that the decay of $g_2(\tau) - 1$ is reasonably well fitted by a single exponential decay, with a relaxation time τ_r that grows with the aging time, increasing by more than two order of magnitudes before possibly starting to level off. A qualitatively similar behavior is found analyzing different ROIs.

In order to compare the aging behavior at long times for different sample locations, it is useful to evaluate the dynamics counting the time, for each single ROI, from the moment when the gel has locally reached a comparable restructuring time. The latter can be consistently stated as the sum of the time t_g when the dynamic arrest takes place with the subsequent characteristic aging time t_a. Fig. 7 shows that the results for τ_r at different ROIs, when plotted as a function of the shifted time $\Delta t(z) = t - [t_g(z) + t_a(z)]$ at the ROI position z, rescale on a single master curve. This means that, to a good approximation, the dynamic evolution of the gel, when referred to Δt, *does not depend on the position along the sample*. This is further confirmed by the inset in the figure, showing that the full correlation functions obtained for different ROIs at the same value Δt superimpose quite well. These observations suggest that, once the gel restructuring reaches a final stage, the microscopic dynamics is spatially homogeneous along the sample and depends only on the "local" age of the gel.

At first sight, a simple exponential form of the correlation functions in a complex system like a gel looks rather surprising. Actually, when colloidal or polymer gels are probed over length scales, set by the inverse scattering wave-vector q^{-1}, which are smaller than the mesh size ξ, $g_2(\tau)$ usually displays a very complex behavior basically reflecting *internal* relaxation processes, which share many aspects in common with the correlation functions observed in glassy systems. However, we probe the gel structure over a length scale of $q^{-1} \simeq 55$ nm,

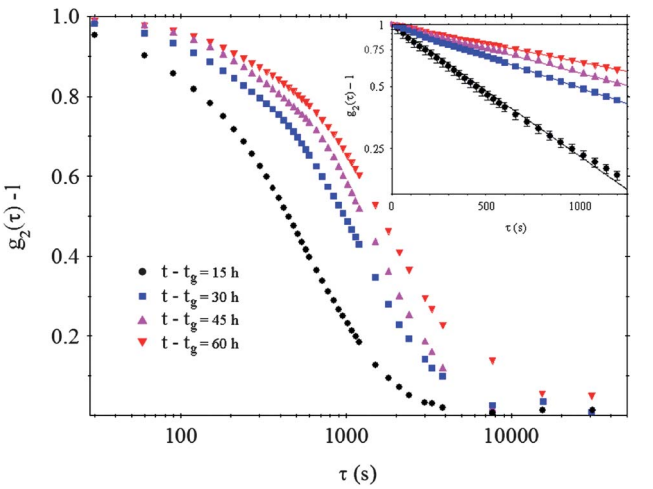

Fig. 6 Correlation functions $g_2(\tau) - 1$ obtained in a fixed ROI located at $z = 0.5$ mm, measured at different aging times $t - t_g$: the semilogarithmic plot in the inset shows that the correlation functions decay roughly exponentially, with a decay constant τ_r that substantially grows with t.

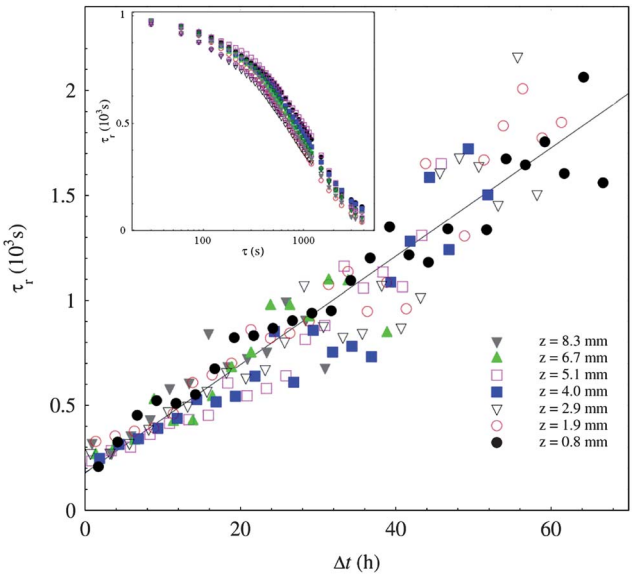

Fig. 7 Microscopic relaxation time τ_r as a function of $\Delta t(h)$ measured with respect to a time-origin $t_g(z) + t_a(z)$, given for each ROI an approximate indication of the instant when the gel has reached an almost stationary structure. The positions along the cell corresponding to the different symbols are specificated in the legend. The inset shows that the full correlation functions obtained for different ROIs at the same value Δt almost superimpose.

which is quite larger than the typical mesh size $\xi = 5$–15 nm of alginate gels.[41] In fact, internal modes, which have typical relaxation times in the range of hundreds of μs[42] (hence 5 orders of magnitude *shorter* than the first delay $\tau_1 = 30$ s measured by PCI), are responsible only for the tiny reduction with respect to the ones in the apparent intercepts of the correlation functions shown in Fig. 6. Notice that the latter, which is already as small as 5% for a relatively "young" gel ($t - t_g = 15$ h), becomes totally negligible as the gel ages.

The very slow dynamics detected by PCI has therefore a radically different physical origin. In the past few years, several experimental and theoretical investigations have indeed suggested that weak colloidal gels and soft glassy systems may exhibit distinctive dynamical features, driven by the accumulation of internal stresses[43–45] generated on a microscopic scale by bond formation and rupture. These stresses relax *via* localized microcollapses creating a long-range elastic deformation field and constituting the elementary steps leading to a progressive gel compaction. On the much longer time scales of such a microscopic stress relaxation, the DLS correlation functions are predicted to behave very differently, both in terms of shape and q-dependence. Whereas the superposition of internal mode relaxations yield a short-time dynamics which is often well described by a stretched exponential,†† $g_2(\tau)$ may display a *compressed* exponential form, namely, the instantaneous decay rate increases with time. A general model based on the relaxation of stress dipoles[44] shows that, provided that the microcollapses take place very rapidly, the behavior of $g_2(\tau)$ is set by a characteristic time scale $\tilde{\tau}_q \simeq \eta(q\xi)/G'$, where G' is the gel compression modulus, and η is the dynamic viscosity. Specifically, $\ln[g(\tau)]$ decays as:

$$\ln[g(\tau)] \sim \begin{cases} (q\tau)^{3/2} & \tau \ll \tilde{\tau}_q \\ q^{3/2}\tau & \tau \gg \tilde{\tau}_q \end{cases} \quad (4)$$

The experimental results for a very weak colloidal gel, with a compression modulus of $G' \simeq 0.1$ mPa, actually support both the compressed exponential form of $g(\tau)$ and the q^{-1} dependence of its decay rate predicted by the upper expression in eqn (4).[43,45] As we shall see in Section 4.2, however, the elastic moduli of the alginate gels we investigate are *hugely* larger, in the range of 10^2 kPa. Hence it is not surprising that the decay of $g_2(\tau)$ is very well fitted by a simple exponential, as predicted by eqn (4) for $\tau \gg \tilde{\tau}_q$. Note that, even in this case, the decay rate should still display a non-diffusive $q^{3/2}$ behavior. Unfortunately, our experimental setup cannot be simply adapted to investigate the q-dependence of $g_2(\tau)$, which might yield an interesting test of the stress-dipole. Nevertheless, when $\ln[g(\tau)] \sim q^{3/2}\tau$, the stress-dipole relaxation model predicts the experimental decay time of $g_2(t)$ to grow linearly with the gel aging time. Fig. 7 shows that indeed, to a good approximation, τ_r increases linearly with Δt in all ROIs, giving an indirect support to the model.‡‡

3.4 Dynamic heterogeneity

The aging of colloidal gels, made of particles linked by short-range attractive interactions, is usually also characterized by a strongly *heterogeneous* dynamics.[28,46] This means that the local degree of correlation at a given time shows strong spatial fluctuations. Moreover, on top of the micro-scale collapses that are supposed to yield the overall decay of the local correlation functions, according to the model described in the former section, the gel aging is characterized also by structural rearrangements witnessed by abrupt decreases of the degree of correlation ("spikes") that extend over wide regions of the sample. The result presented in what follows show that a very similar behavior is shared by alginate polymer gels with physical cross-links. Studying gels characterized by an aging stage varying along the z direction allows us to investigate by PCI how the degree spatial and temporal heterogeneity qualitatively and quantitatively depends on aging.

Striking evidence of the sudden rearrangements characterizing the heterogeneous dynamics of aging alginate gels can be obtained by focusing on a single structural rearrangement event visualized by means of a so-called "dynamical activity map", where the spatial distribution of the correlation index is represented by a false-color map.[47] In order to clearly point out that dynamic heterogeneity occurs not only along the aging direction, but also at constant z (namely, within gel regions that are supposed to be structurally homogeneous, at least on the average), it is useful to re-define the subdivision of the sample into regions of interest as follows. A first ROI in the speckle pattern is constructed as a 15 px × 15 px square. Then, all the other ROIs are generated by shifting the latter by 5 px along either the z-axis or the horizontal coordinate x. Besides yielding

†† For a discussion of this functional behavior, see Section 4.2.

‡‡ Note that, when $\ln[g(\tau)] \sim (q\tau)^{3/2}$, one would rather expect $\tau_r \sim (\Delta t)^{2/3}$.

a much clearer visualization, this method, although introducing some correlation between adjacent partially overlapping ROIs, can be shown to ensure better spatial resolution. To each of these regions is then attributed the average value of the normalized correlation index $\hat{c}_I(\tau;t,\boldsymbol{r})$ within the ROI, evaluated at the delay time $\tau = 30$ s. Fig. 8 shows a typical sequence of maps referring to a *single* rearrangement event. In the first map, referring to a starting time $t = t^*$ just before the rearrangement occurs, a fully correlated region (in red), where the sample is already dynamically arrested, can be clearly told apart from a fully uncorrelated zone (in blue) close to the top of the observation region, where gelation has not yet taken place. Moreover, a decrease of the degree of correlation by increasing z witnesses the different aging stages within the gel phase. In the second activity map, taken at starting times $t^* + \tau$, a rearrangement event generating close to the gel interface is seen to turn the *whole* gel into a dynamically active structure that almost completely looses correlation within a delay time τ, showing that the events rapidly propagate over macroscopically large length scales. Subsequently, correlation is recovered starting from the bottom, more "aged" part of the gel, until, at $t \simeq t^* + 3\tau$ the gel reverts to a state that does not substantially differ from the original one. The possibility that these correlation drops are not artifacts due to a rigid motion of the speckle field,[28] generated for instance by a sudden detachment of the gel from the cell walls as a consequence of a macroscopic shrinkage, can be easily ruled out by an image correlation velocimetry analysis.[22] As already mentioned, gel shrinking effects can conversely be clearly detected after gelation has taken place over the whole sample.

These results, together with those discussed in Section 3.3, suggest that there are two kinds of dynamic processes taking place in an aging alginate gel: a progressive slowing down of the local microscopic dynamics, witnessed by the increase of the structural relaxation time τ_r, and an intermittent sequence of restructuring "bursts", involving the whole sample but not leaving any significant trace on the gel structure, at least apparently. These two different processes are better appreciated by considering the time behavior of the fluctuations in c_I, expressed by its (coarse-grained) variance $\chi(\tau)$. As discussed in Section 2, this amounts to evaluating how much the degree of correlation after a delay time τ fluctuates over the pixels in a given ROI, taking than the average of the standard deviation of c_I over a short time window δt. In the two panels of Fig. 9, which refer to two ROIs at different vertical positions z, the behavior of χ as a function of τ is represented by a single vertical line of thickness δt with a color code that varies from blue to red with an increasing value of $\chi(\tau)$, whereas the way $\chi(\tau)$ changes with the time t after sample preparation is monitored on the horizontal axis. On both ROIs, the structural rearrangements leading to the slowing down of the local microscopic dynamics are associated with a strong increase of $\chi(\tau)$ at short delays τ, lasting for a significant fraction of the aging time t_a. Since both t_g and t_a depend on z, both the temporal location and the duration of this process are considerably different for the two ROIs. A more detailed analysis shows that $\chi(\tau)$ is peaked around the value of the structural relaxation time τ_r at time t, whereas the amplitude of the peak progressively decreases with τ. Conversely, after the main structural rearrangement on spatial scales of the order of q^{-1} has completed (namely, for $t > t_a$ when the local dynamics has reached the quasi-homogenous stage shown in Fig. 7), sudden increases of $\chi(\tau)$ lasting for a time $t \leq \delta t$, but persisting for much longer delays τ, take place. Since these events correspond to de-correlation bursts rapidly propagating over the whole sample, they take place at the *same* time on the two ROIs, namely, their timing is not dictated by the local aging stage, but only on the *absolute* time t.

Such a temporal coincidence of the de-correlation bursts on different sample regions is strikingly highlighted by Fig. 10, where a time window of about 20 h, beginning at $t > t_g + t_a$, is shown for five different ROIs along the sample. Notice that the time interval between two consecutive drops increases with the aging time. The evolution of the gel towards a more homogeneous state, witnessed for $t - t_g < t_a$ both by the behavior of the local dynamics and by the fading of the fluctuations in c_I, is then also accompanied by a later progressive decrease of the frequency of global rearrangements persisting for a very long time. Although the timing of the global de-correlation events is the

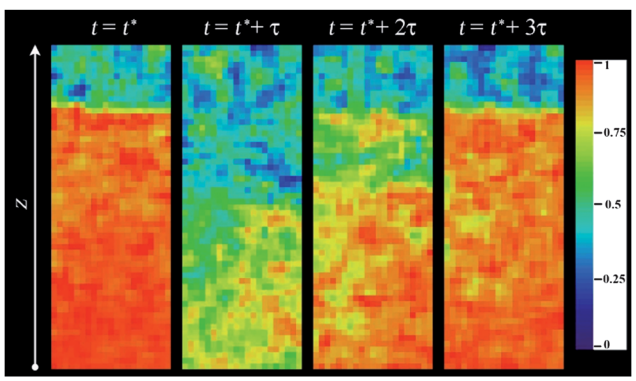

Fig. 8 Sequence of activity maps, obtained as described in the text, referring to a single restructuring event taking place at a time $t^* \simeq 40$ h after sample preparation. The scale to the right displays the color scale for the normalized degree of correlation $\hat{c}_I(30\text{ s};t,\boldsymbol{r})$.

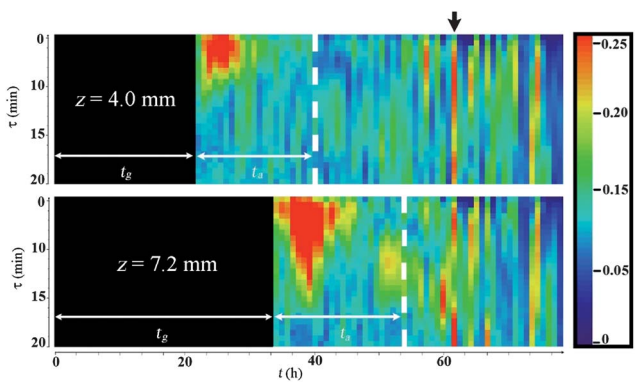

Fig. 9 Dependence on the delay time τ (vertical axis) of the standard deviation $\chi(\tau)$ of the correlation index, shown in the color code, as a function of time t. The two graphs refer to different ROIs displaying the indicated gelation and aging times t_g, t_a. The arrow points at a typical abrupt de-correlation burst.

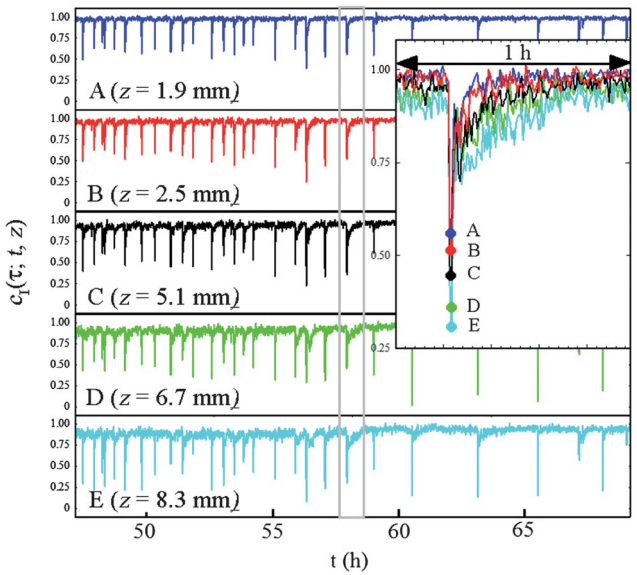

Fig. 10 Coincident "spiking" behavior of $c_I(\tau;t,z)$ for five different ROIs over a time window of about 20 h. The inset shows the superposition of the spiking events occurring between the two grey lines in all the ROIs.

same over the whole gel, the amplitude and duration of a single spike on a *specific* ROI depends on the aging stage of the latter. The inset in Fig. 10 shows indeed that the bursts get stronger and longer with z. This means that the sample regions where the gel is relatively "younger" are more affected by the rearrangement and take more time to revert to their original state.

4 Mechanical properties of the gels

The alginate gels whose macroscopic properties we investigated were prepared according to a procedure which had to necessarily be quite different from the way gelation was obtained in the PCI experiments. Here gelation proceeds from the membrane inwards, hence the longitudinal compression measurements performed at a given aging time reflect only the average mechanical properties of gels whose structure varies along the radial direction. This amounts to testing simultaneously a set of parallel "springs" whose elastic constants physically correspond to gels at diverse aging stages. The compression and stress relaxation tests discussed in this section are not therefore meant to provide a full mechanical characterization of alginate gels, but rather to support qualitatively our microscopic PCI investigation. Nonetheless, our preliminary data already bear clear evidence of the progressive overall aging of the gel structure, and yield further hints on the nature and kinetics of cross-links in alginate gels.

4.1 Uniaxial compression tests

We first discuss the results of uniaxial compression tests obtained as described in Section 2 for alginate solutions kept in the gelation bath for a period of time ranging between 6 h, roughly corresponding for the selected experimental geometry to the minimum time required to obtain a macroscopic weak gel, and 144 h. The samples were compressed at constant speed from an initial length h_0 to a final length h, and the uniaxial compression stress σ_m in excess of the pre-stress value defined in Section 2 was measured as a function of the strain $\lambda = 1 - h/h_0$. The experimental excess stress σ_m was then corrected for the increase of gel cross-section at a constant volume to obtain the "true" stress $\sigma = \sigma_m(1 - \lambda)$. The double-log plot in the inset of Fig. 11 shows that the overall stress–strain relationships for different aging times t progressively merge into a single curve, characterizing the region where a consistent strain hardening is observed. With the exception of the samples kept in the gelation bath for 6 h, the maximum compression that the gels can sustain before rupture is almost independent of t. An expanded linear view of the different curves of $\sigma(\lambda)$ for a compressional strain not exceeding $\lambda \simeq 0.2$, shown in the main body of Fig. 11, first displays a linear increase of $\sigma(\lambda)$ (full lines), corresponding to a Young's modulus $E = \sigma/\lambda$ that steadily increases from $E \simeq 150$ kPa to $E \simeq 350$ kPa with increasing gelation time. This linear elastic region (region I) is limited however to compression values not exceeding about 5%, and is followed by a roll-off rapidly leading to a behavior which is still linear, but corresponds to an apparent elastic constant $E' \simeq 120$ kPa which is almost independent of sample aging (region II). The lower-right inset shows that the intercept σ_0 of the linear fits (dotted lines) with the $\lambda = 0$ axis, corresponding to an apparent yield stress, grows roughly linearly with the gel Young's modulus E measured at small compression values. While the behavior at small λ shows that the gel stiffens with t, for a sufficiently large deformation the time spent in the gelation bath seems to affect the alginate gels only for what concerns σ_0, whereas their apparent compression modulus does not change.

The latter observation, together with the merging of all the response curves in the strain hardening region, suggests that the gel elastic response at small λ may stem from the

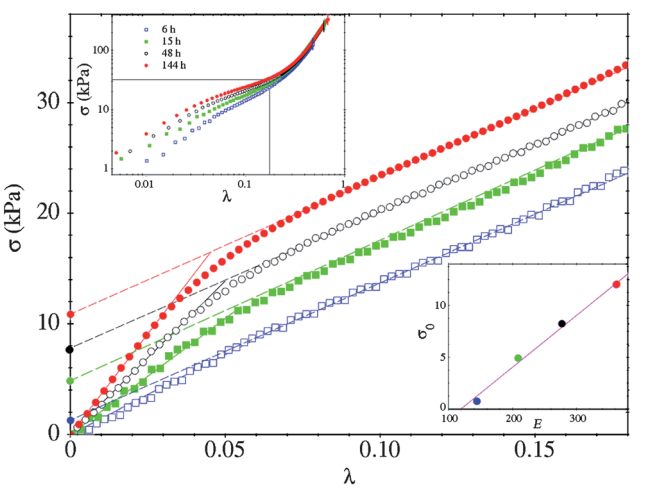

Fig. 11 Upper-left inset: uniaxial stress–strain relationship for alginate gels made by permeation of a 0.1 M calcium chloride solution for the periods of time t shown in the legend, obtained at a compression speed of 1 mm s^{-1}. Vertical bars indicate the maximum compression that each sample can bear before gel rupture. Each curve is obtained as the average of at least four samples obtained under the same conditions. Main body: expanded linear view. The boxed region, extending up to a maximum compression of about 20%. Lower-right inset: linear behaviour of the apparent yield stress σ_0 with the gel's Young's modulus E.

concurrence of more microscopic mechanisms, whereas larger deformations are controlled by a single mechanism, not affected by t. A similar behavior has been recently observed in gels made of synthetic alginates where the fractional content of GM alternating sequences can be carefully controlled by Mørch *et al.*,[48] who pointed out that the gels display a degree of plasticity that increases with the length of the alternating GM blocks, very probably due to the restructuring of the junctions involving GM sequences. On the basis of this evidence, the observed stress–strain behavior can be accounted for by assuming that the crosslinks between GG sequences form at the early stages of the gelation process and are weakly affected both in number and strength by gel ripening, whereas additional links due to GM sequences increase in number and strength with aging, increasing the overall stiffness of the gel. Because the latter cross-links are weaker, they are more easily subject to breaking under stress than pure guluronate cross-links, so that, by increasing λ, the gel evolves from a state where its elastic response is due by both kinds of links to an intermediate pseudo-plastic state where the apparent Young's modulus is determined by the stiff GG bonds alone. Moreover, the separation between two different elastic regimes should be much more pronounced for more aged gels, in agreement with the experimental evidence (in fact, it is almost negligible at $t = 6$ h, when the inner part of the gel has barely formed).

Such a different behavior of the two kinds of cross-links for what concerns their rates of formation and breaking can arguably be justified by the specific features of calcium binding to alginate, which takes place in three separate steps:[49] Ca^{2+} ions first interact with a single guluronate unit to form ion–monomer complexes, which then pair to generate egg-box dimers eventually associating into bond sequences. Whereas the kinetic rate of the first step clearly does not depend on the kind of link that is formed, in the case of GG blocks, the following ones are however strongly cooperative due to the specific stereochemistry described by the egg-box model. In fact long sequences of paired GG blocks can form at a much faster rate.[48] Hence, the GG binding sites presumably get saturated as soon as the gelation front runs into them, while the subsequent gel ripening entails a slow spatial rearrangement of the GG junctions, but not their increase in number and strength. Conversely the cross-links formed by alternating GM sequences, which are known to be much less stereospecific,[18] grow at a much slower rate, progressively strengthening a basic framework mostly made of GG bonds. In this picture, rather large GG junctions are then seen as stiff, permanent blocks embedded into an elastic medium whose global elastic properties evolve however with the gel aging, because they depend on the number and strength of GM bonds too. The latter, which break and restructure much more easily than the large GG cross-link sequences,[18] actually provide an efficient way to relax local stresses in the gel. The presence of this weaker, easily restructuring links, is then likely to play a crucial role in determining the peculiar mechanical properties of a physical polymer gel like alginate.[13]

Let us briefly comment on the eventual strain-hardening behaviour of alginate gels at very large values of λ, which is actually shared by many other biopolymer gels. In the case of thin and flexible F-actin and intermediate filament networks, strain hardening may be accounted for by a nonlinear force-extension behavior of the individual filaments leading to a uniform affine deformation of the structure.[1,50] Conversely, the response of a network consisting of stiff thick fibers, such as collagen and bundled actin, seems to be governed by collective bending deformations.[51–54] Because it contains very large cross-link regions, often exceeding the size of the chain segments between two junctions, an alginate gel may be regarded as a kind of composite, simultaneously displaying the presence of stiff and soft regions.[55] The non-linear elastic behavior of this composite polymer network has started to be investigated only recently.[13] When the volume fraction of the stiff component is so low that it does not form a percolating network, strain hardening can be accounted for by modeling the system as a fiber-reinforced elastic composite, where the cross-link regions are regarded as stiff rods randomly and isotropically distributed in a softer matrix.[56–58] Such a composite model, however, does not take into account the most peculiar property of polymer gels characterized by physical cross-links with a finite lifetime such as alginate, namely, that the network topology is unceasingly fluctuating because the cross-links continuously break and reform at different locations. The experimental consequences of this ceaseless network dynamics is discussed in the next section.

4.2 Stress relaxation

At a compression speed of 1 mm s^{-1}, therefore, the gel responds to a uniaxial compression with a finite stress, displaying an overall behavior that, in regions I and II, resembles that of a "pseudo-plastic" solid. However, both the full decay of the correlation functions measured by PCI and the persistence of large scale restructuring bursts, witnessing that the microscopic dynamics never stops, suggest that the gel may actually creep macroscopically over a very long time, so that its mechanical response should be regarded as *truly* plastic. In other words, one may wonder whether the gel would actually *yield* when deformed at an infinitesimally slow rate. This question is better answered by testing the value after a delay τ of the stress $\sigma(\tau)$ after a given compression has been rapidly applied at $\tau = 0$, for samples kept in the gelation bath for increasingly longer periods of time t. Here we present only the results obtained in the limits of a very short or very long t and to a single value $\lambda = 0.1$ of the initially applied strain, which roughly correspond to the initial part of region II in Fig. 11, where, according to our tentative interpretation, most of the GM cross-links have already opened up. This does not mean, however, that the weaker GM bonds should not contribute to stress relaxation, for novel cross-links of this kind may re-form and break while the sample relaxes.

A first clear evidence that can be extracted from the stress relaxation measurements shown in Fig. 12 is that the stress $\sigma(\tau)$ (made dimensionless by normalizing to its initial value) always decays asymptotically to zero, even for the largest curing time $t = 144$ h. Thus, in the long time limit, all gels yield and comply to the applied strain, which actually implies a fully plastic behavior at vanishingly small compression rates. Hence, the

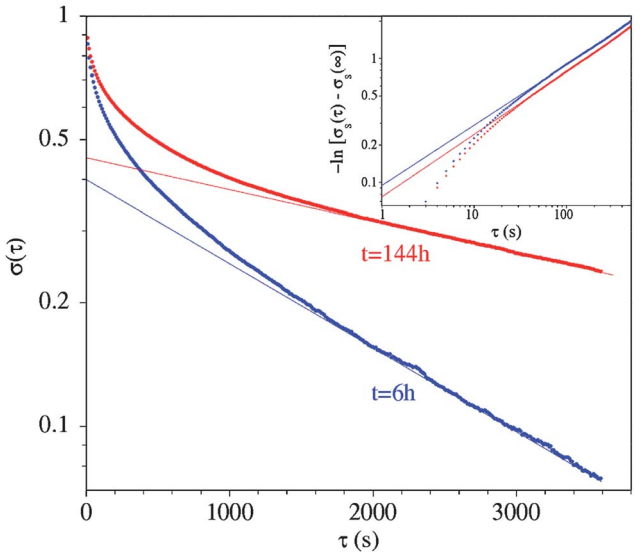

Fig. 12 Main body: normalized stress σ, as a function of the delay time τ after a compression of 10% was rapidly applied, for samples kept in the gelation bath for 6 h and 144 h. Inset: negative logarithm $-\ln[\sigma_s(\tau) - \sigma_s(\infty)]$ of the short-time relaxations, obtained as discussed in the text, fitted with stretched exponentials in the range 50 s $\leq \tau \leq$ 500 s. The best-fit parameters are $\beta = 0.47$, $\tau_{\sigma s} = 115$ s for $t =$ 6 h, and $\beta = 0.49$, $\tau_{\sigma s} = 150$ s for $t = 144$ h.

stress–strain relationship depends on the compression rate, so that alginate gels behave in fact as *thixotropic* materials, albeit their creeping behavior is extremely slow. The semi-log plot shows that, at long delay time τ, the normalized stress displays a simple exponential decay

$$\sigma(\tau) \xrightarrow[t\to\infty]{} \sigma_l(\tau) \sim \exp\left(-\tau/\tau_{\sigma_l}\right), \tag{5}$$

where the long-time stress decay constant $\tau_{\sigma l}$ increases from about 2100 s for the weak gel kept in the gelation bath for just 6 h, to 5600 s for the most aged gel. Quite interestingly, these values are of the same order of magnitude of the microscopic relaxation time τ_r of the correlation functions in aged gels. The microscopic stress-relaxation model we used in Section 3.3 to account for the time behavior of $g_2(\tau)$ suggests a physical picture of the long-time creeping behavior of the gel expressed by eqn (5), possibly providing an explanation of the close similarity between $\tau_{\sigma l}$ and τ_r. The decrease in $\sigma(\tau)$, which is in fact a decrease in the pressure felt by the compressing plate due to gel yielding, is of course related to a progressive reduction of the overall gel strain $\lambda(t)$ through the stress–strain experimental relationship shown in Fig. 11, which deviates only moderately from linearity. If we assume that the macroscopic strain relaxation results from the addition of a large number of uncorrelated microscopic collapses occurring at random points in the gel, $\lambda(t)$ would be a Poisson process, exponentially decaying with the *same* time constant of the local correlation.

At short time, however, the strain relaxation curve is significantly non-exponential, displaying in particular an extremely steep decay for $\tau \to 0$, witnessing that, at short time, very fast relaxation mechanisms contribute to $\sigma(\tau)$ too. Stress relaxation curves are commonly fitted with an arbitrary superposition of exponentials that, however, are very hard to be attributed to specific physical mechanisms. It is conversely tempting to try to give an overall description of $\sigma(\tau)$ that, albeit approximate, may be related to a general physical picture. As a first guess, the long time contribution to the stress relaxation given by eqn (5) may be tentatively factorized out by writing

$$\sigma(\tau) = \sigma_l(\tau)\sigma_s(\tau). \tag{6}$$

This amounts to assuming that the mechanism responsible for the long-time creeping of the gel is totally uncorrelated with the microscopic mechanisms contributing to the fast initial decay of $\sigma(\tau)$. This is a rather crude approximation, which however yields a short-time contribution that of course *does not* decay to zero, but to a *finite* value $\sigma_s(\infty) \simeq 0.4$ for both curves, a behavior actually expected for a fully arrested gel. Interestingly, by subtracting from $\sigma_s(\tau)$ its long-time plateau value both curves behaves very similarly and can be accurately fitted, except at very small τ, by a "stretched-exponential" (SE) function

$$\sigma_s(\tau) - \sigma_s(\infty) = \exp[-(\tau/\tau_{\sigma_s})^{\beta}] \tag{7}$$

where τ_{σ_s} is a characteristic time constant, and the exponent $\beta \leq 1$ accounts quantitatively for the amount of "stretching", lower values of β corresponding to a function that at short time decay much faster than a simple exponential with the same decay constant τ_{σ_s}, displaying however a much longer long-time tail. This behavior is better appreciated by plotting the (negative) logarithm of $\sigma_s(\tau) - \sigma_s(\infty)$. A pure stretched exponential yields indeed a power-law behavior $-\ln[\sigma_s(\tau) - \sigma_s(\infty)] = (\tau/\tau_{\sigma_s})^{\beta}$, which on a double log plot appears as a straight line with a slope β. As shown in the inset in Fig. 12), this is actually the case for $\tau \gtrsim$ 30–50 s. Moreover, both curves show an almost *identical* stretch exponent $\beta \simeq 0.5$, and close values of $\tau_{\sigma_s} \simeq$ 100–150 s.§§

SE relaxations are observed frequently in a multitude of different physical situations ranging from the microscopic dynamics of supercooled liquids and spin glasses,[59,60] to the response of critical mixtures and polymer solutions to external fields.[61,62] One of the reasons for the ubiquity of this functional behavior is because a SE behavior naturally emerges as the long-time asymptotic behavior of the superposition of parallel relaxation mechanisms that depend on a continuous parameter ℓ and individually yield an exponential decay with a time constant $\tau(\ell)$, provided that the probability distribution of these different mechanisms has the very general form $P(\ell) \sim \exp[-(\ell/\ell_0)^p]$.[63] In particular, when $\tau(\ell)$ scales as ℓ^q, the stretch exponent is given by $\beta = p/(p+q)$. Since in our general picture the gel, initially subjected to an external stress, relaxes by the sequential breaking of cross-links of the alginate chains that can have widely different lengths ℓ and bond strengths, an overall SE relaxation of $\sigma_s(\tau)$ is not too surprising. Borrowing

§§ A better estimate of the overall decay constant of the SE relaxation is given by its time integral $\langle\tau\rangle = \int_0^\infty d\tau \exp[-(\tau/\tau_{\sigma_s})^{\beta}] = \beta^{-1}\Gamma(\beta^{-1})\tau_{\sigma_s}$, Γ being the gamma function, yielding $\langle\tau\rangle \simeq 260$ s at $t = 6$ h and $\langle\tau\rangle \simeq 310$ s at $t = 144$ h. The fact that $\langle\tau\rangle$ is more than one order of magnitude smaller than $\tau_{\sigma l}$ confirms a clear separation of the time scales for the short and long time relaxations.

some basic concepts commonly used in describing stress relaxation in biopolymer bundles,[6,64] we assume that breaking a bond of size made of ℓ individual Ca^{2+} links requires an activation energy $E_a(\ell)$ linearly proportional to ℓ and the local longitudinal compressional force F the bond feels,[64] which is directly related to the macroscopically applied stress. In a first approximation, the time τ_b it takes to cross the barrier and break the bond is given by the product of the Boltzmann factor of $E_a(\ell)$ times the equilibrium lifetime of a *single* link τ_b^{eq} in the absence of an external load,[6] $\tau_b(\ell) = \tau_b^{eq}\exp(F\ell/k_BT)$. Hence, assuming that bonds of a specific size ℓ lead to a single exponential decay of the stress proportional to $\exp[-\tau/\tau_b(\ell)]$ (so that $q = 1$), a stretched exponential decay with $\beta \simeq 1/2$ would result from an exponentially decaying ($p = 1$) probability distribution for the bond size ℓ or, approximately, even if $P(\ell)$ is a Poisson distribution with a low average value $\langle\ell\rangle$. Although rather heuristic, this simple superposition model provides some clues for the origin of the short-time SE behavior of the stress relaxation in terms of local rearrangements.

5 Conclusions and perspectives

Our results show that polymer networks like those formed by alginate by the addition of a bivalent electrolyte, inducing the cooperative formation of non-covalent, reversible bonds made by a variable number of ionic links, share many features in common with physical colloidal gels. Specifically, the gel displays a complex aging behavior, characterized by a strongly heterogeneous microscopic dynamics involving both local rearrangements persisting over very long time, and collective restructuring effects evidenced by sudden de-correlation bursts. At variance with simple colloidal gels, however, the specific ionic nature of the cross-links in alginate yields a network which is never fully arrested, always showing a fully decaying behavior of the local time-correlation functions. Moreover, the slow gel formation induced by the perfusion of the curing agent displays a peculiar non-diffusive advancement of the gelation front, which might possibly be due to micro-convective effects, followed by a slow reinforcement of the network, ascribable to the formation of novel bonds and the restructuring of the existing ones. A basic investigation of the macroscopic mechanical response of the gel, both as a function of the applied strain and as a function of time following an initial rapid deformation, supports the basic picture derived from the investigation of the microscopic dynamics. In particular, the slow creeping behavior of the gel observed after a first rapid stress relaxation, which can be attributed to the concurrence of many superpositions of local relaxation modes yielding an overall SE decay, is consistent with the persistence of a local microscopic diffusive dynamics over long times and with the occurrence of intermittent global rearrangements.

The simultaneous presence of stronger, stereospecific bonds, provided according to the egg-box model by the GG sequences, with the weaker links, which breaks and re-forms much more easily, provided by the alternate GM sequences, seems to be crucial to induce the long-time creeping behavior of alginate gels. A detailed analysis of the distinct role played by these two kinds of links and their specific contribution to the dynamics and macroscopic rheology of alginate gels would be better performed by investigating synthetic alginates, where the amount and distribution of the GG and GM sequences can be carefully controlled, as described in the seminal study made by Mørch *et al.*[48] Nonetheless, a basic test of their different roles can also be performed by gelling alginate in the presence of a consistent amount of a monovalent, neutral electrolyte like NaCl. Whereas the presence of such an additive would not influence too much the strongly stereospecific bounds provided by the GG sequences, unless at very high ionic strength, the Na^+ cations would indeed favorably compete with calcium in binding to the GM sites, strongly hindering their propensity to form cross-links.[18] Several experimental investigations of the macroscopic properties of alginate gels in the presence of neutral electrolytes seem to support this view.[36,65] Preliminary gelation experiments actually show that, in the presence of an amount of NaCl as low as 0.1 M, the microscopic dynamics is drastically modified. In particular, the gel gets fully arrested, the restructuring kinetics also changes. Consistently, the macroscopic creeping of the gel is totally suppressed. A full analysis of electrostatic effects on the microscopic dynamics of alginate gels will be the subject of forthcoming publications.

References

1 C. Storm, J. Pastore, F. MacKintosh, T. Lubensky and P. Janmey, *Nature*, 2005, **435**, 191–194.
2 Y. Fung, *Biomechanics: mechanical properties of living tissues*, Springer, 1993, vol. 12.
3 O. Chaudhuri, S. Parekh and D. Fletcher, *Nature*, 2007, **445**, 295–298.
4 X. Trepat, L. Deng, S. An, D. Navajas, D. Tschumperlin, W. Gerthoffer, J. Butler and J. Fredberg, *Nature*, 2007, **447**, 592–595.
5 O. Lieleg, M. Claessens and A. Bausch, *Soft Matter*, 2010, **6**, 218–225.
6 O. Lieleg, J. Kayser, G. Brambilla, L. Cipelletti and A. Bausch, *Nat. Mater.*, 2011, **10**, 236–242.
7 A. Bausch and K. Kroy, *Nat. Phys.*, 2006, **2**, 231–238.
8 C. Semmrich, T. Storz, J. Glaser, R. Merkel, A. Bausch and K. Kroy, *Proc. Natl. Acad. Sci. U. S. A.*, 2007, **104**, 20199.
9 B. Kim, J. Nikolovski, J. Bonadio and D. Mooney, *Nat. Biotechnol.*, 1999, **17**, 979–983.
10 W. Pilnik and F. Rombouts, *Carbohydr. Res.*, 1985, **142**, 93–105.
11 A. D. Augst, H. J. Kong and D. Mooney, *Macromol. Biosci.*, 2006, **6**, 623.
12 O. Smidsrød, *J. Chem. Soc., Faraday Trans.*, 1974, **57**, 263.
13 J. Sun, X. Zhao, W. Illeperuma, O. Chaudhuri, K. Oh, D. Mooney, J. Vlassak and Z. Suo, *Nature*, 2012, **489**, 133–136.
14 E. Morris, D. Rees, D. Thom and J. Boyd, *Carbohydr. Res.*, 1978, **66**, 145–154.
15 K. Potter, B. Balcom, T. Carpenter and L. Hall, *Carbohydr. Res.*, 1994, **257**, 117–126.
16 I. Donati, S. Holtan, Y. Mørch, M. Borgogna, M. Dentini and G. Skjåk-Bræk, *Biomacromolecules*, 2005, **6**, 1031–1040.

17 Y. Zhao, F. Hu, J. Evans and M. Harris, *Chem. Eng. Sci.*, 2011, **66**, 848–858.
18 I. Donati, Y. Mørch, B. Strand, G. Skjåk-Bræk and S. Paoletti, *J. Phys. Chem. B*, 2009, **113**, 12916–12922.
19 M. Mancini, M. Moresi and R. Rancini, *J. Food Eng.*, 1999, **39**, 369–378.
20 L. Wolff, P. Fernandez and K. Kroy, *New J. Phys.*, 2010, **12**, 053024.
21 K. Lee, M. Peters, K. Anderson and D. Mooney, *Nature*, 2000, **408**, 998–1000.
22 G. Brambilla, S. Buzzaccaro, R. Piazza, L. Berthier and L. Cipelletti, *Phys. Rev. Lett.*, 2011, **106**, 118302.
23 H. Grasdalen, *Carbohydr. Res.*, 1983, **118**, 255–260.
24 L. Cipelletti, H. Bissig, V. Trappe, P. Ballesta and S. Mazoyer, *J. Phys.: Condens. Matter*, 2003, **15**, S257.
25 S. Maccarrone, G. Brambilla, O. Pravaz, A. Duri, M. Ciccotti, J. Fromental, E. Pashkovski, A. Lips, D. Sessoms, V. Trappe, *et al.*, *Soft Matter*, 2010, **6**, 5514–5522.
26 L. Berthier, G. Biroli, J. Bouchaud, L. Cipelletti, D. El Masri, D. L'Hôte, F. Ladieu and M. Pierno, *Science*, 2005, **310**, 1797–1800.
27 P. Tokumaru and P. Dimotakis, *Exp. Fluids*, 1995, **19**, 1–15.
28 A. Duri, H. Bissig, V. Trappe and L. Cipelletti, *Phys. Rev. E: Stat. Phys., Plasmas, Fluids, Relat. Interdiscip. Top.*, 2005, **72**, 051401.
29 A. Mikkelsen and A. Elgsaeter, *Biopolymers*, 1995, **36**, 17–41.
30 R. Liesegang, *Naturwiss. Wochenschr.*, 1896, **11**, 353.
31 T. Witten Jr and L. Sander, *Phys. Rev. Lett.*, 1981, **47**, 1400–1403.
32 G. Barkema, M. Howard and J. Cardy, *Phys. Rev. E: Stat. Phys., Plasmas, Fluids, Relat. Interdiscip. Top.*, 1996, **53**, 2017–2020.
33 L. Gálfi and Z. Rácz, *Phys. Rev. A*, 1988, **38**, 3151.
34 S. Cornell, Z. Koza and M. Droz, *Phys. Rev. E: Stat. Phys., Plasmas, Fluids, Relat. Interdiscip. Top.*, 1995, **52**, 3500.
35 Z. Koza, *J. Stat. Phys.*, 1996, **85**, 179–191.
36 B. Thu, O. Gåserød, D. Paus, A. Mikkelsen, G. Skjåk-Bræk, R. Toffanin, F. Vittur and R. Rizzo, *Biopolymers*, 2000, **53**, 60–71.
37 T. Braschler, A. Valero, L. Colella, K. Pataky, J. Brugger and P. Renaud, *Anal. Chem.*, 2011, **83**, 2234–2242.
38 J. Thumbs and H. Kohler, *Chem. Phys.*, 1996, **208**, 9–24.
39 R. Piazza, S. Buzzaccaro and E. Secchi, *J. Phys.: Condens. Matter*, 2012, **24**, 284109.
40 A. Kiselev and L. Ryzhik, *Ann. Henri Poincare C*, 2001, **18**, 309–358.
41 J. Klein, J. Stock and K. Vorlop, *Eur. J. Appl. Microbiol. Biotechnol.*, 1983, **18**, 86–91.
42 K. A. Strand, A. Bere, P. S. Dalberg, T. Sikkeland and O. Smidsrød, *Macromolecules*, 1982, **15**, 570–579.
43 L. Cipelletti, S. Manley, R. C. Ball and D. A. Weitz, *Phys. Rev. Lett.*, 2000, **84**, 2275–2278.
44 J. Bouchaud and E. Pitard, *Eur. Phys. J. E*, 2001, **6**, 231–236.
45 A. Duri and L. Cipelletti, *Europhys. Lett.*, 2006, **76**, 972–978.
46 H. Bissig, S. Romer, L. Cipelletti, V. Trappe and P. Schurtenberger, *PhysChemComm*, 2003, **6**, 21–23.
47 A. Duri, D. Sessoms, V. Trappe and L. Cipelletti, *Phys. Rev. Lett.*, 2009, **102**, 085702.
48 Y. Mørch, S. Holtan, I. Donati, B. Strand and G. Skjåk-Bræk, *Biomacromolecules*, 2008, **9**, 2360–2368.
49 Y. Fang, S. Al-Assaf, G. Phillips, K. Nishinari, T. Funami, P. Williams and L. Li, *J. Phys. Chem. B*, 2007, **111**, 2456–2462.
50 M. Gardel, J. Shin, F. MacKintosh, L. Mahadevan, P. Matsudaira and D. Weitz, *Science*, 2004, **304**, 1301–1305.
51 O. Lieleg, M. Claessens, C. Heussinger, E. Frey and A. Bausch, *Phys. Rev. Lett.*, 2007, **99**, 88102.
52 D. Chen, Q. Wen, P. Janmey, J. Crocker and A. Yodh, *Annu. Rev. Condens. Matter Phys.*, 2010, **1**, 301–322.
53 M. Sheinman, C. Broedersz and F. MacKintosh, *Phys. Rev. E: Stat. Phys., Plasmas, Fluids, Relat. Interdiscip. Top.*, 2012, **85**, 021801.
54 P. Onck, T. Koeman, T. van Dillen and E. van der Giessen, *Phys. Rev. Lett.*, 2005, **95**, 178102.
55 J. Zhang, C. Daubert and E. Allen Foegeding, *J. Food Eng.*, 2007, **80**, 157–165.
56 E. Huisman, C. Heussinger, C. Storm and G. Barkema, *Phys. Rev. Lett.*, 2010, **105**, 118101.
57 C. Broedersz, C. Storm and F. MacKintosh, *Phys. Rev. Lett.*, 2008, **101**, 118103.
58 M. Das and F. MacKintosh, *Phys. Rev. Lett.*, 2010, **105**, 138102.
59 W. Gotze and L. Sjogren, *Rep. Prog. Phys.*, 1992, **55**, 241.
60 B. Castaing and J. Souletie, *J. Phys.*, 1991, **1**, 403.
61 R. Piazza, T. Bellini, V. Degiorgio, R. Goldstein, S. Leibler and R. Lipowsky, *Phys. Rev. B: Condens. Matter*, 1988, **38**, 7223.
62 V. Degiorgio, R. Piazza, F. Bellini, T. Mantegazza and R. E. Goldstein, *Phys. Rev. Lett.*, 1990, **64**, 1043.
63 M. A. Continentino and A. P. Malozemoff, *Phys. Rev. B: Condens. Matter*, 1986, **33**, 3591.
64 R. Vink and C. Heussinger, *J. Chem. Phys.*, 2012, **136**, 5102.
65 M. LeRoux, F. Guilak and L. Setton, *J. Biomed. Mater. Res.*, 1999, **47**, 46–53.

